THE JOURNAL OF BIOLOGICAL CHEMISTRY
Vol. 278, No. 15, Issue of April 11, pp. 13110–13117, 2003
Printed in U.S.A.

NMR Study of Mersacidin and Lipid II Interaction in Dodecylphosphocholine Micelles

CONFORMATIONAL CHANGES ARE A KEY TO ANTIMICROBIAL ACTIVITY*

Received for publication, October 31, 2002, and in revised form, January 23, 2003
Published, JBC Papers in Press, January 31, 2003, DOI 10.1074/jbc.M211144200

Shang-Te D. Hsu‡, Eefjan Breukink§, Gabriele Bierbaum¶, Hans-Georg Sahl¶, Ben de Kruijff§, Rob Kaptein‡, Nico A. J. van Nuland‡, and Alexandre M. J. J. Bonvin‡‖

From the ‡NMR Department, Bijvoet Center for Biomolecular Research and §Biochemistry of Membranes, Center for Biomembrane and Lipid Enzymology, Utrecht University, 3584CH, Utrecht, The Netherlands and the ¶Institute of Medical Microbiology and Immunology, University of Bonn, D-53015 Bonn, Germany

Mersacidin belongs to the type B lantibiotics (lanthionine-containing antibiotics) that contain post-translationally modified amino acids and cyclic ring structures. It targets the cell wall precursor lipid II and thereby inhibits cell wall synthesis. In light of the emerging antibiotics resistance problem, the understanding of the antibacterial activity on a structural basis provides a key to circumvent this issue. Here we present solution NMR studies of mersacidin-lipid II interaction in dodecylphosphocholine (DPC) micelles. Distinct solution structures of mersacidin were determined in three different states: in water/methanol solution and in DPC micelles with and without lipid II. The structures in various sample conditions reveal remarkable conformational changes in which the junction between Ala-12 and Abu-13 (where Abu is aminobutyric acid) effectively serves as the hinge for the opening and closure of the ring structures. The DPC micelle-bound form resembles the previously determined NMR and x-ray crystal structures of mersacidin in pure methanol but substantially deviates from the other two states in our current report. The structural changes delineate the large chemical shift perturbations observed during the course of a two-step ^{15}N-^{1}H heteronuclear single quantum coherence titration. They also modulate the surface charge distribution of mersacidin suggesting that electrostatics play a central role in the mersacidin-lipid II interaction. The observed conformational adaptability of mersacidin might be a general feature of lipid II-interacting antibiotics/peptides.

Many antimicrobial peptides act against microorganisms through pore formation on the cell membrane. The permeability originates in principle from a nonspecific assembly that results in a pore-like structure where the amphipathic nature of the amino acid composition facilitates the clustering process (for a review, see Ref. 1). Apart from this ubiquitous mechanism, some antimicrobial peptides, such as ramoplanin, enduramycin, and janiemycin and the glycopeptides vancomycin and teicoplanin, use specific targets that play a central role in the cell wall synthesis, namely lipid II, to achieve their bioactivity with much higher efficiency (2–4). Lipid II also serves as a target for the pore-forming peptides nisin and epidermin, which belong to the type A lantibiotic (lanthionine-containing antibiotic) family (2, 5). Some type B lantibiotics also possess functions of targeted cell wall synthesis inhibition; one of the best studied peptide is mersacidin (see Fig. 1*A*) (6, 7). Although these lipid II-targeting antimicrobial peptides share a common binding molecule, the recognition epitopes among these peptides are somewhat different: co-incubation of vancomycin or other inhibitors of transglycosylases or transpeptidases with mersacidin does not impede their lipid II binding capacity (6). As antibiotic resistance is becoming more and more severe, the diversity of such a targeting action is of great interest. The sophisticated chemical composition of lipid II provides the complexity that can be targeted in various ways. It consists of a peptidoglycan head group that serves as the building block for the cross-linked cell wall matrix and of a pyrophosphate-undecaprenyl lipid tail that functions as the carrier for the transport of the peptidoglycan moiety from the cytoplasm to the extracellular domain (see Fig. 1*B*). Although the targeted antimicrobial activity of mersacidin is evident, little detail is known, however, about its mechanism of recognition and inhibition.

Mersacidin is a 20-residue peptide with nine post-translationally modified amino acids and a single negatively charged residue, Glu-17 (Fig. 1*A*) (for reviews, see Refs. 8 and 9). It contains four ring structures: two separate ones in the N-terminal part and two intertwined ones in the C-terminal part. The three-dimensional structure of mersacidin has been solved both by solution NMR spectroscopy (10) and x-ray crystallography (11). Unlike type A lantibiotics, which are mostly extended and flexible, the structure of mersacidin is globular and compact. In both the crystalline and solution states the local ring structures are tightly confined by the lanthionine linkages. The overall conformations obtained from the two different methods are similar except for a minor difference in the orientation of the glycine-rich ring (residues 5–11). These structures were, however, both solved in pure methanol, due to the poor solubility of mersacidin in aqueous solution, and in the absence of lipid II, which is required for its bioactivity. To understand the mechanism of action of mersacidin, knowledge of its structure upon binding to lipid II under physiological conditions is crucial.

We report here high resolution NMR spectroscopy studies of the interaction between mersacidin and its binding target lipid

* The costs of publication of this article were defrayed in part by the payment of page charges. This article must therefore be hereby marked "*advertisement*" in accordance with 18 U.S.C. Section 1734 solely to indicate this fact.

The atomic coordinates and structure factors (code 1MQX, 1MQY, and 1MQZ) have been deposited in the Protein Data Bank, Research Collaboratory for Structural Bioinformatics, Rutgers University, New Brunswick, NJ (http://www.rcsb.org/).

The assigned chemical shift data sets were deposited into the BioMagResBank under accession codes 5581, 5582, and 5580.

‖ To whom correspondence should be addressed. Tel.: 31-30-2533859; Fax: 31-30-2537623; E-mail: abonvin@nmr.chem.uu.nl.

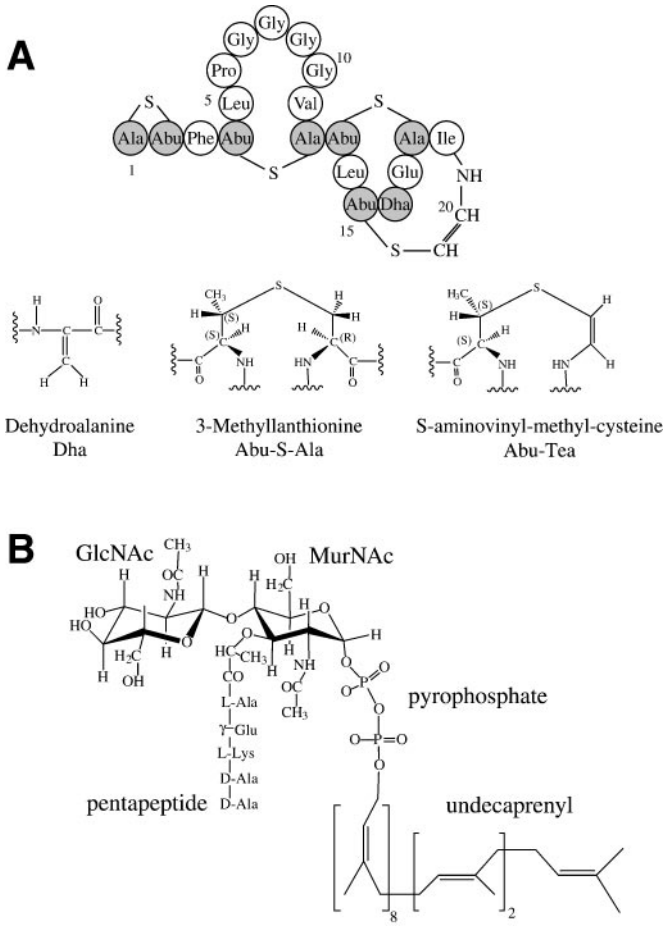

FIG. 1. **Primary structures of mersacidin (*A*) and lipid II (*B*).** *A*, post-translationally modified amino acids are highlighted in *gray*, and their chemical structures are depicted below. *B*, GlcNAc, *N*-acetylglucosamine; MurNAc, *N*-acetylmuramic acid.

II in dodecylphosphocholine (DPC)[1] micelles, which were used as a membrane mimic. ^{15}N-^{1}H HSQC titration experiments provide residue-specific insight into the interaction with lipid II. The solution NMR structures of mersacidin in various sample environments, namely free in methanol/water solution and DPC-bound in the absence and presence of lipid II, are presented. The effect of binding to DPC micelles and lipid II on the mersacidin dynamics are characterized by means of ^{15}N relaxation together with gradient-edited diffusion experiments. Despite the large number of published solution NMR structural and relaxation dynamics studies of membrane proteins and peptides (12–16), only a few examples of high resolution NMR studies of protein/peptide-ligand interactions in the presence of membrane-like environments are available to date (17, 18). We will show that the differences in sample environments result in substantial conformational changes that modulate the charge accessibility. These changes in charge distributions most likely play a crucial role in the mechanism of mersacidin bioactivity.

MATERIALS AND METHODS

Sample Preparation—For the overproduction and purification of [^{15}N]mersacidin, the producer strain *Bacillus* sp. HIL Y-85,54728 was inoculated into 10 ml of tryptone soy broth and incubated overnight. The preculture served as inoculum for 10 ml of synthetic production medium (19), which contained 50 mM $^{15}NH_4Cl$ (>98%) (Cambridge Isotope Laboratories, Inc., Cambridge, UK) and 10 mM K_2SO_4. It was incubated at 30 °C to an optical density of 0.1 at 600 nm. 0.1 ml of this culture served as inoculum for 10 100-ml cultures in the same medium that were incubated for 72 h at 30 °C with vigorous agitation in 1-liter Erlenmeyer flasks. The culture supernatant was sterilized by filtration and loaded onto a 50-ml Serdolit PAD-I column (Serva Electrophoresis GmbH, Heidelberg, Germany), which had been washed with methanol and equilibrated with distilled water. The column was washed with 10 bed volumes of distilled water and 10 bed volumes of 50% methanol in 50 mM potassium phosphate, pH 7, and the peptide was eluted with 500 ml of acetonitrile, 0.1% trifluoric acid. The antibacterial activity of the fractions was checked in a bioassay using *Micrococcus luteus* ATCC 4698 as an indicator strain. Active fractions were pooled and concentrated by rotary evaporation, and precipitated proteins were removed by centrifugation. Aliquots of the concentrate were applied to a POROS 20 R2 HPLC column (Applied Biosystems, Weiterstadt, Germany) using the following gradient (eluent A: 0.1% trifluoric acid in water, eluent B: 0.1% trifluoric acid in acetonitrile): 0 min 5% B, 12 min 30% B, 20 min 40% B, 22 min 100% B at a flow of 5 ml/min. Active fractions were pooled, concentrated by evaporation, and rechromatographed on the POROS column. After lyophilization of the active fractions, the peptide was applied to a reversed phase HPLC column (RP18) using the following gradient: 0 min 5% B, 30 min 50% B, 44 min 67.5% B, 47 min 100% B. The mass of the purified peptide, which eluted at 55% B, was checked by mass spectrometry. Lipid II was prepared as described previously (7).

NMR Spectroscopy for Spectral Assignments—Due to the solubility problem of mersacidin, freeze-dried mersacidin was first dissolved in perdeuterated d_3-methanol (Cambridge Isotope Laboratories, Inc.) as a 10 mg/ml stock solution. It was then diluted with sodium phosphate buffer and DPC solution and water. Lipid II was taken from a stock solution (in $CHCl_3$:MeOH = 1:1) and vacuum-dried before mixing. Mersacidin-containing DPC solution was then added to dissolve lipid II, and the resulting sample solution was transferred into an NMR tube for measurements. A short sonication was applied after each mixing step to ensure uniform mixing and proper micelle formation. The typical sample concentration was 2 mM mersacidin in 10 mM sodium phosphate buffer at pH 6.0 with a total volume of 500 μl. The sample hence contained 37% methanol and 63% H_2O. For structure determination purposes, 4% (~100 mM) perdeuterated d_{38}-DPC (Cambridge Isotope Laboratories, Inc.) with or without 2 mM lipid II was added to obtain lipid II embedded in DPC micelles and a control sample of mersacidin in DPC micelles alone. For simplicity, MeOH/H_2O, DPC_{bound}, and lipid II are defined here as the three sample conditions of free mersacidin in the methanol/water mixture and in the DPC micelle solution with and without lipid II, respectively.

All NMR experiments were carried out on Varian UnityPlus 500 and Bruker DRX600 and DRX750 spectrometers at 293 K. Spectra including two-dimensional NOESY with mixing times of 50, 100, and 200 ms, a total correlation spectroscopy with mixing time of 70 ms, and a three-dimensional NOESY-HSQC with mixing time of 100 ms were collected to obtain complete backbone and side chain proton resonance assignments (21). A two-dimensional double quantum filtered correlation spectroscopy was recorded to extract the backbone $^{3}J_{HN\text{-}H\alpha}$ coupling constants in combination with a short mixing time (50 ms) NOESY as described previously (22). Stereospecific assignment of side chain methylene groups was achieved based on the intensity correlations of the spin systems (23–25). All spectra were processed using the NMRPipe software package (26) and analyzed with NMRView (27) except for those of diffusion measurements (see below). The assigned chemical shift data sets of mersacidin in three different conditions, MeOH/H_2O, DPC_{bound}, and lipid II, were deposited into the BioMagResBank under accession codes 5581, 5582, and 5580, respectively.

Two-step ^{15}N-^{1}H HSQC Titration Experiments—For the starting point corresponding to the free mersacidin in the 37% MeOH, 63% H_2O mixture, 1 μmol of the ^{15}N-labeled mersacidin stock solution in d_3-methanol was diluted with 50 μl of 100 mM sodium phosphate buffer, and water was added to reach a total volume of 450 μl. In the first titration step, aliquots of a 40% DPC stock solution with 37% methanol content were successively added resulting in DPC concentrations of 0.2, 1, 2, 3, 4, 5, and 6%. This is respectively equivalent to a range of ratios of mersacidin *versus* DPC micelles of 20:1 up to 1:1.5, assuming that each DPC micelle consists of 50–55 monomers (28, 29). At the end of the first titration step (DPC_{bound}) the total volume was 525 μl resulting in a 16% sample dilution but with identical methanol content. For the second titration step, portions of 0.05, 0.25, 0.5, 0.75, 1, 1.25, and 1.5

[1] The abbreviations used are: DPC, dodecylphosphocholine; HPLC, high pressure liquid chromatography; HSQC, heteronuclear single quantum coherence; NOE, nuclear Overhauser effect; NOESY, nuclear Overhauser effect spectroscopy; PFG, pulse field gradient; Dha, dehydroalanine; Abu, aminobutyric acid; Tea, *S*-aminovinyl-methyl-cysteine; SAS, solvent-accessible surface; r.m.s.d., root mean square deviation.

μmol of vacuum-dried lipid II were first prepared in separate containers and then successively dissolved in the sample taken from the NMR tube to reach the same concentration ratios as those of the DPC titration steps. The final sample (lipid II) therefore contained 1 μmol of [^{15}N]mersacidin, ~1.5 μmol of DPC micelles and 1.5 μmol of lipid II. In both titration steps, the chemical shift changes of mersacidin were all saturated by an excess of DPC micelles and lipid II at a 1:1.25 molar ratio and higher.

^{15}N Relaxation Experiments for Backbone Dynamics—^{15}N longitudinal relaxation times T_1, transverse relaxation times T_2, and ^{1}H-^{15}N steady-state NOEs of mersacidin were obtained from series of two-dimensional experiments with coherence selection achieved by pulse field gradients (PFGs) (30). For T_1 measurements, seven spectra were recorded with relaxation delays T set to 10, 20, 100, 300, 500, 750, and 1000 ms. For the rotating frame relaxation times $T_{1\rho}$, spectra were first obtained using a ^{15}N spin lock continuous wave radio frequency (rf) with a field strength ν_1 of 1 kHz for seven relaxation delays T of 20, 50, 70, 100, 120, 200, and 350 ms. The relaxation times T_1 and $T_{1\rho}$ were then derived from a single exponential decay fitting of the peak intensities using *xcrfit* (www.pence.ca/ftp/xcrvfit). The T_2 of each residue was subsequently derived from the observed relaxation time $T_{1\rho}$ by correcting for the offset $\Delta\nu$ of the rf field to the resonance by use of the relation $1/T_{1\rho} = (1/T_1)\cos^2\theta + (1/T_2)\sin^2\theta$, where $\theta = \tan^{-1}(\nu_1/\Delta\nu)$. ^{1}H-^{15}N heteronuclear NOEs were determined from the ratio of peak intensities (I^{on}/I^{off}) with and without the saturation of the amide protons for 3 s. All ^{15}N relaxation experiments were carried out on a Varian UnityPlus 500 spectrometer at 293 K.

Since the structure of mersacidin exhibits high flexibility, quantitative analysis of the relaxation data in terms of spectral density functions is not applicable (31). Therefore, the relaxation data in the three different sample conditions were only compared in a qualitative way. A further simplification allows us to estimate the correlation time from the averaged T_2 value (32) according to Equation 1,

$$\tau_c \sim 1/(5T_2) \quad \text{(Eq. 1)}$$

The overall correlation time can also be expressed as a function of the molecular size and the bulk solvent viscosity η. For a spherical molecule of radius a rotating in a liquid of viscosity η, the rotational correlation time τ_c is given by the Stokes relation (33) according to Equation 2,

$$\tau_c = 4\pi a^3\eta/3kT = V\eta/kT = 1/6D_{rot} \quad \text{(Eq. 2)}$$

where V is the volume of the molecule, k is the Boltzman constant, T is the absolute temperature, and D_{rot} is the rotational diffusion constant for a spherical molecule. The molecular radius a is actually the effective hydrodynamic radius R_h of the molecule with the hydration shell. The overall correlation time estimated from NMR relaxation measurements can thus be compared with the effective molecular size and sample viscosity that are measured from PFG-NMR diffusion experiments.

Pulse Field Gradient NMR Diffusion Experiment—The hydrodynamic radius R_h can be calculated from the translational diffusion coefficient D_{trans} of the particles through another Stokes relation according to Equation 3,

$$D_{trans} = kT/6\pi\eta R_h \quad \text{(Eq. 3)}$$

PFG-NMR diffusion measurement with the PG-SLED (pulse gradient-stimulated echo longitudinal encode-decode) sequence enables us to obtain D_{trans}, which is proportional to the decay rate d of the NMR signal attenuation as a function of gradient strength g (34), according to Equation 4,

$$I(g) = I_o\exp[-dg^2] \quad \text{(Eq. 4)}$$

where I_o is the NMR peak intensity in the absence of gradient pulses and g is the field strength of the bipolar gradient pulse pair. Changes in the solvent viscosity η in different sample environments can be monitored using the methanol signal as an internal standard, assuming that methanol does not interact with other solutes and thus that its hydrodynamic radius R_h is invariable in analogy to the use of dioxane for protein folding studies as described previously (34). The ratio of the rate constants of methanol in different conditions gives the relative change in bulk solvent viscosity η. Knowing this, the relative hydrodynamic radii R_h of mersacidin with respect to methanol in different environments can thus be extracted. In practice, each diffusion data set consists of a series of 40 one-dimensional ^{1}H spectra with 2.5% increments of the gradient strength from 2.5 to 100% collected at 750 MHz with a three-axis gradient probe (x axis for bipolar gradient pulse pair and y and z axis for residual signal crushing). Data processing was performed with Felix from Biosym Technologies (San Diego, CA), and Origin7.0 from OriginLab (North Hampton, MA) was used for non-linear fitting to obtain the translational diffusion coefficients D_{trans}.

Structure Calculation and Analysis—All structure calculations were performed with the program CNS (35) using the ARIA setup and protocols (36). Semiautomated NOE assignment was used to assist the spectral assignment (37). This was done from a partially assigned NMRView peak list. The initially unassigned cross-peaks were defined as ambiguous distance restraints with a lower weighing factor. The calibration of the cross-peak intensities against distances was done automatically at the beginning of each iteration. The additional unambiguously assigned cross-peaks were interactively re-examined with NMRView, and the checked peak list was then used as the input for the next calculation in an iterative way until all cross-peaks were assigned. Each semiautomated assignment step with ARIA consisted of eight iterations with successive reduction of the violation tolerance and a final refinement in explicit solvent using default ARIA parameters unless otherwise stated. The Parallhdg5.3 force field with the PROLSQ parameters was used (38). The topologies of dehydroalanine (Dha), aminobutyric acid (D-Abu), 3-methyllanthionine, and the cyclized C terminus of the *S*-aminovinyl-methyl-cysteine (Tea) were constructed based on alanine, threonine, and cysteine and comparison of available data bases. Four thioether bridges were introduced. Nine backbone ϕ and four side chain χ_1 torsion angle restraints obtained from the stereospecific assignments of the methylene groups of the thioester-linked Ala-12 and Ala-18 and of Leu-14 and Glu-17 were used in the structure calculations. A torsion angle dynamics simulated annealing protocol was performed, initially at 10,000 K (8000 steps), followed by a first cooling stage to 50 K (50 K/step); Cartesian space refinement was used for the second cooling stage (from 2000 to 1000 K in 16,000 steps) and the subsequent third cooling stage (from 1000 to 50 K in 4000 steps) followed by 200 steps of energy minimization. The slow cooling process at the second stage ensures a better convergence of the calculated structures. The 50 structures with the lowest restraint energy were further subjected to explicit solvent refinement (OPLS water and Me_2SO models) as described previously (39), and the best 20 were kept for clustering and structural analysis. A cluster is defined as a group of at least four structures with pairwise backbone (residue 3, 4, and 12–20) positional root mean square deviations (r.m.s.d.) lower than 0.3 Å. Structures were visualized and analyzed with MOLMOL (40). DynDom was used to identify conformational changes and to define domains and effective hinge regions of the structures obtained under the three different sample conditions (41). The coordinates of the three structure ensembles, MeOH/H_2O, DPC_{bound}, and lipid II, were deposited in the Research Collaboratory for Structural Bioinformatics Protein Data Bank under accession codes 1MQX, 1MQY, and 1MQZ, respectively.

RESULTS

Substantial Chemical Shift Changes Indicate a Strong Dependence of the Mersacidin Conformation on Its Environment—The assignment of the resonances of mersacidin in various sample environments was achieved by a standard multidimensional NMR protocol using the ^{15}N-labeled sample (21). A two-step ^{15}N-^{1}H HSQC titration of perdeuterated DPC micelles followed by unlabeled lipid II was then used to investigate the interaction of mersacidin and lipid II. Chemical shifts are excellent probes for biomolecular interaction studies because of their sensitivity to the changes in the surrounding chemical environment. They are commonly used for the mapping of ligand binding sites in proteins (42), and yet, as will be discussed later, the chemical shift perturbations upon ligand binding can also be governed by structural rearrangements. The first step (DPC micelles) was used as a control to monitor how mersacidin was influenced by the membrane-mimicking environment. Both sequential titration experiments revealed significant chemical shift perturbations in mersacidin (Fig. 2). The addition of DPC micelles strongly affects the backbone amide protons of Gly-7, Abu-13, Abu-15, and Glu-17 in the ^{1}H dimension (mainly upfield shifts) and most of the C-terminal part in the ^{15}N dimension (Fig. 3). Along the ^{15}N dimension, a downfield shift occurs at Dha-16, which is flanked by progressively increasing, almost symmetric, upfield shifts. Subsequent addition of lipid II gives rise to large downfield shifts for the

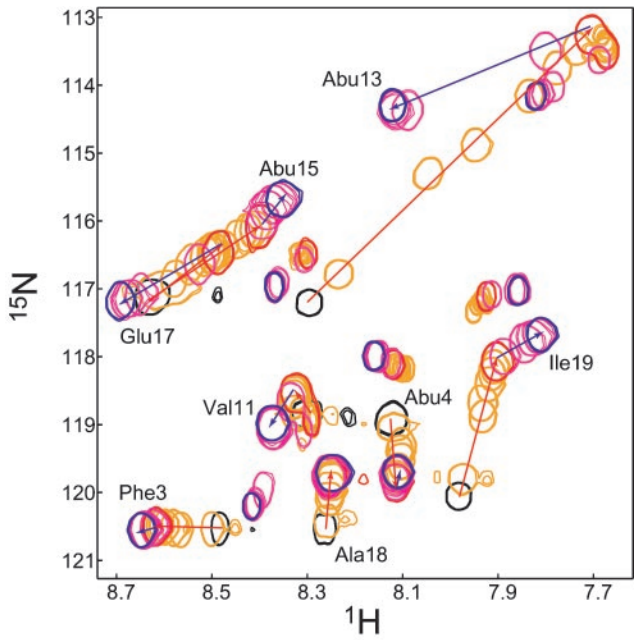

FIG. 2. **Representative spectral region of the two-step ^{15}N-^{1}H HSQC titration experiments of DPC micelles and lipid II at 293 K, 500 MHz.** *Black*, starting point, MeOH/H_2O; *red*, the end point after DPC titration, DPC_{bound}; *blue*, the second end point after lipid II titration, lipid II. Directions of chemical shift changes are shown in *red* (MeOH/H_2O → DPC_{bound}) and *blue* (DPC_{bound} → lipid II). The intermediate titration steps (5, 25, 50, 75, 100, and 125% mersacidin concentration) are shown in *orange* and *magenta* for DPC micelles and lipid II, respectively.

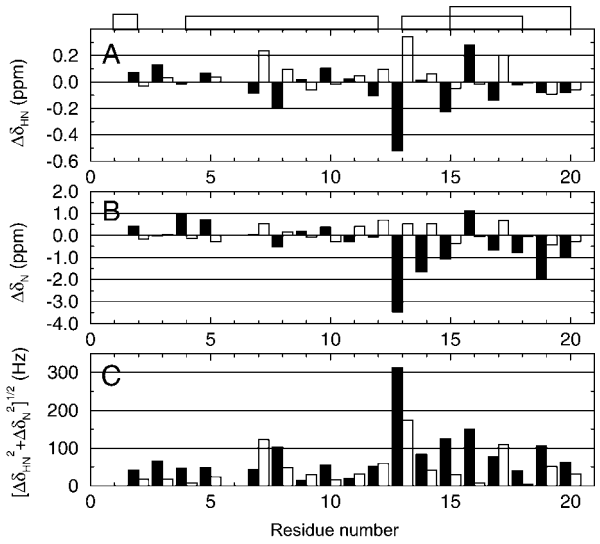

FIG. 3. **Chemical shift perturbation as a function of the primary sequence of mersacidin upon successive addition of DPC micelles (*filled bars*) and lipid II (*open bars*).** *A*, ^{1}H chemical shift perturbation ($\Delta\delta_{HN}$). *B*, ^{15}N chemical shift perturbation ($\Delta\delta_N$). *C*, absolute displacements ($[(\Delta\delta_{HN})^{2n}+(\Delta\delta_N)^2]^{1/2}$) in Hz from HSQC spectra collected at 500 MHz. The lanthionine linkages are depicted by *lines* on the *top panel*.

amide protons of Gly-7, Abu-13, and Glu-17 in the ^{1}H dimension; a similar chemical shift perturbation profile is observed in the ^{15}N dimension. The general direction of change is, however, inverted compared with the first DPC micelles titration. Both titration steps result in clearly localized effects. Unlike the strong binding affinity between nisin and lipid II, which results in slow exchange cross-peak patterns in similar titration experiments (18), mersacidin follows a fast exchange profile indicative of weaker binding under these conditions. The gradual changes in position can easily be followed during the course of both titration processes (Fig. 2). Unexpectedly the addition of DPC micelles seems to affect mersacidin more than its specific target, lipid II, does. The titration data suggest an interesting interconversion process. For Gly-7, Gly-8, Ala-12, Abu-13, and Glu-17, the ^{1}H chemical shifts first move upfield and then conversely shift downfield. A similar behavior is monitored along the ^{15}N dimension for most residues, *e.g.* Glu-17. Since chemical shifts are closely related to the surrounding chemical environment primarily defined by the three-dimensional structure, the direction and displacement of the cross-peaks suggest that the structure of mersacidin undergoes a substantial change upon addition of DPC micelles and is somehow restored close to its initial conformation, if not identical, upon the subsequent addition of lipid II. Yet this could also be an indication that mersacidin falls off the DPC micelles after addition of lipid II and is restored to a state similar to the initial condition (free mersacidin in MeOH/H_2O).

Binding-induced Overall Backbone Relaxation Dynamics Changes—To confirm that mersacidin remains bound to DPC micelles upon titration of lipid II, we performed ^{15}N-^{1}H relaxation experiments in conjunction with diffusion experiments to examine the dynamics and molecular size of the complexes. NMR ^{15}N-^{1}H relaxation experiments have been extensively applied to proteins to study the dynamics of protein motions within a wide range of time scales (43–45). Changes in protein dynamics upon ligand binding can be extracted from the relative differences before and after binding. For example, shortened T_2 and increased ^{15}N-^{1}H NOEs upon ligand binding are indicative of a rigidification of, for example, a flexible loop. It should be noted that the relaxation parameters are also closely associated to the molecular weight. In the case of binding interactions, the increased molecular weight of the overall complex will affect the relaxation parameters of each component globally. This effect can be particularly pronounced when a small peptide binds to large micelles (14). In our case, the molecular weight of DPC micelles is roughly 10 times higher than that of mersacidin and lipid II. During the titration process, mersacidin binds to DPC micelles and lipid II, and hence its apparent molecular weight is considerably increased. The relaxation dynamics analysis in the three different states, namely MeOH/H_2O, DPC_{bound}, and lipid II, reveals indeed a uniform increase of the plateau of the ^{1}H-^{15}N heteronuclear NOEs and longitudinal relaxation times T_1 and a decrease of the transverse relaxation times T_2 as a result of large complex formation (Fig. 4). These data also reflect the dynamics of the local structures. The similar sequential patterns observed in the three states indicate no particular stabilization of local structure upon binding; local motions still exist. In all states, the glycine-rich ring exhibits higher flexibility as indicated by the lower ^{1}H-^{15}N heteronuclear NOEs and longer T_2 with respect to the average values. In contrast, the residues that are linked by lanthionine linkages, Abu-4, Ala-12, Abu-13, Abu-15, Ala-18, and Tea-20, exhibit higher ^{1}H-^{15}N heteronuclear NOE and shorter T_2 (Fig. 4). Overall the most stable structure elements are the segments that are connected by the glycine-rich ring (residues 4–5 and 12–14), their backbone motion being obviously restricted by their ring structures.

The increases of effective molecular size and bulk solvent viscosity can both contribute to the global change in relaxation parameters (33). Therefore, PFG-NMR diffusion experiments were used to discriminate between those. In such experiments, the change of solution viscosity can be monitored independently by using a separate internal probe, in our case, methanol (see "Material and Methods") (34). The addition of DPC micelles and lipid II increased the solvent viscosity by 7.4 and

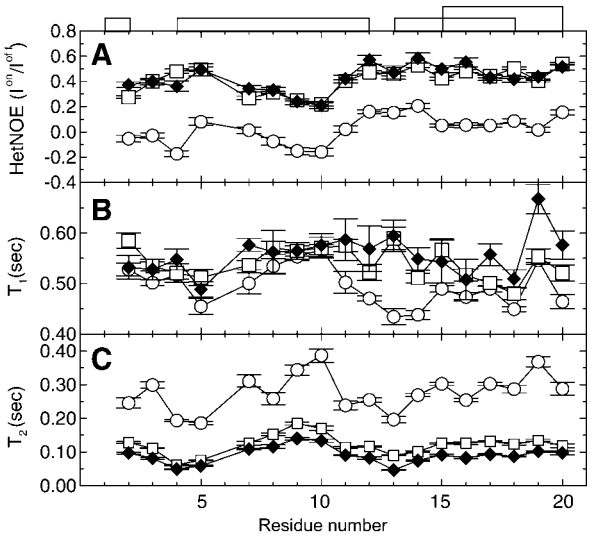

FIG. 4. **^{15}N relaxation dynamics parameters of mersacidin.** *A*, ^{1}H-^{15}N heteronuclear NOE (*HetNOE*). *B*, longitudinal relaxation time T_1. *C*, transverse relaxation time T_2. *Open circles* (○), MeOH/H_2O; *open squares* (□), DPC_{bound}; *filled diamonds* (♦), lipid II. The standard deviations are shown by *bars*. The lanthionine linkages are depicted on the *top panel*.

6.7%, respectively. This is significantly less than the 22.9 and 26.1% increases of the translational diffusion coefficient ratio of mersacidin and methanol upon addition of DPC micelles and subsequently lipid II, respectively (Table I). This can only be explained by an increase of the effective molecular size due to the binding to DPC micelles and lipid II. A good correlation is obtained between the overall tumbling rates τ_c estimated from T_2 relaxation and from diffusion experiments ($R^2 = 0.86$). This confirms that mersacidin binds to DPC micelles and remains bound in the presence of lipid II and that the resulting decrease of the overall tumbling rate is at the origin of the observed global effect on the relaxation parameters.

Solution NMR Structures Reveal Dramatic Conformational Changes—Fig. 5 summarizes the observed proton-proton contacts in mersacidin derived from NOESY spectra recorded under different sample conditions. The NOE contact maps in the three different conditions show similar patterns with only a few variations, suggesting that the topology of mersacidin does not alter much upon changes in the environment. Some long range NOEs are absent in MeOH/H_2O, *e.g.* between Phe-3 and Glu-17, and some variation occurs in the glycine-rich ring under all three conditions. These small differences in NOE contacts reflect, however, remarkable conformational changes. Fig. 6 shows the ensemble of structures obtained from structure calculation based on the NOEs derived from the NOESY spectra recorded in different environments. The intertwined ring structure provides a well defined backbone structure in the C-terminal part (residue 13–20) in all conditions, although MeOH/H_2O deviates slightly from DPC_{bound} and lipid II. The N terminus and the glycine-rich ring are less defined due to the fact that the glycine repeat is prone to low NOE density as well as local flexibility. Two populations of the glycine-rich ring for the lipid II-bound form are found after clustering (named L2a and L2b). These two clusters have identical backbone conformations except for the glycine residues: two distinct ring conformations are observed with their planes flipped by almost 180° with respect to each other. Since they both satisfy all distance restraints, they were both kept for structural comparisons.

Among all three conditions, the DPC micelle-bound form (DPC_{bound}) is the best defined in terms of r.m.s.d. of the ensemble and the most favorable in terms of total energy after explicit solvent refinement (Table II). The structures contain no conventional secondary structure element because of their unusual post-translationally modified amino acids. To evaluate the effect of solvent hydrophobicity onto the structure (methanol and DPC are both hydrophobic, and this can affect especially the side chain packing), two types of solvent models (water (hydrophilic) and Me_2SO (hydrophobic)) were used for structure refinement. The results show no distinguishable difference both in structure and in energy (data not shown). In both cases, the electrostatic energy term is dominant, and the DPC_{bound} structures have the lowest electrostatic energies. The main structural difference occurs in the relative orientation of the glycine-rich ring with respect to the intertwined rings. The addition of DPC micelles induces a large amplitude twisting of 162° of those rings with Abu-13 and Leu-14 as the effective hinge (Fig. 7). The subsequent addition of lipid II in the presence of DPC micelles then induces an inverse twist (100° for L2a and 167° for L2b) that results in conformations close to the initial state. The hinge region, centered at Abu-13, experiences a dramatic change in its chemical environment that is reflected in the chemical shift changes during the course of the ^{15}N-^{1}H HSQC titrations. The same conformational change directly affects the electrostatic energy since the distance between the two sole charged groups (N terminus and Glu-17 side chain) is modulated by this twisting motion. This becomes clear when looking at the surface electrostatic potentials (Fig. 8). DPC_{bound} highly resembles the structure that was previously solved in the crystalline state in pure methanol. The N terminus and Glu-17 side chain in MeOH/H_2O point toward two opposite sides, while the two charged groups come close to each other as a result of the twist induced by DPC micelles, which obviously lowers the electrostatic energy (Table II).

Comparison of the structures of mersacidin with and without lipid II in DPC micelles has revealed intriguing conformational changes. While the hydrophobicity of DPC micelles induces the closure of the structure, in contrast, the addition of lipid II results in the exposure of the charged groups (Fig. 8). The exposure of the Glu-17 side chain can be quantitatively monitored from its change in solvent-accessible surface (SAS) area. The addition of DPC micelles reduces the SAS area from 155 Å^2 (MeOH/H_2O) to ~55 Å^2 (DPC_{bound}), and the addition of lipid II increases again the SAS area to about the same value of 155 Å^2 (L2a and L2b). The positively charged N terminus of Ala-1, undergoes similar changes in SAS area with almost identical values (data not shown). Another significant but inverse change occurs at Ile-19 with a 60% increase in SAS area upon the addition of DPC micelles (from 100 to 160 Å^2) and a drop to 80 Å^2 when lipid II is present. In addition to the dramatic changes in side chain packing and charge distribution, the backbone structure is also affected when DPC micelles are added to free mersacidin. Notable differences in backbone torsion angles for Abu-2, Phe-3, Abu-4, Ala-12, Abu-13, Leu-14, and Abu-15 are monitored between the free (MeOH/H_2O) and the DPC micelle-bound form (DPC_{bound}), while subsequent addition of lipid II (L2a and L2b) does not induce much more changes (data not shown). These differences are consistent with the observed ^{15}N chemical shift changes, which are indicative for backbone conformational changes. Large changes occur in the N- and C-terminal parts when DPC micelles are added, and much smaller changes are found when lipid II is added (Fig. 3). Although the opening of the structure increases the electrostatic energy of mersacidin *per se*, the binding interface and in particular the interaction with its counterpart, lipid II, must compensate for the energetic cost of exposing the two charges in the hydrophobic micelle environment (Table II).

TABLE I
Translation diffusion parameters obtained from PFG-NMR experiments

	$MeOH/H_2O$	DPC_{bound}	Lipid II
Decay rate constant[a]			
$d^{methanol}$	15.04	14.00	14.09
$d^{mersacidin}$	2.04	1.55	1.52
Relative increase of bulk solvent viscosity (%)[b]			
$(\eta^i/\eta^{MeOH/H_2O}) - 1$	0	7.4	6.7
Relative hydrodynamic radius			
$R_h^{mersacidin}/R_h^{methanol}$	7.35	9.03	9.27

[a] The decay rate constant d is obtained from Gaussian fitting of the attenuated NMR signals as a function of the fractional gradient strength g using Equation 4.
[b] The increase of bulk solvent viscosity η can be derived from the observed decay rate constants for methanol and is inversely proportional to their ratios (see "Material and Methods").

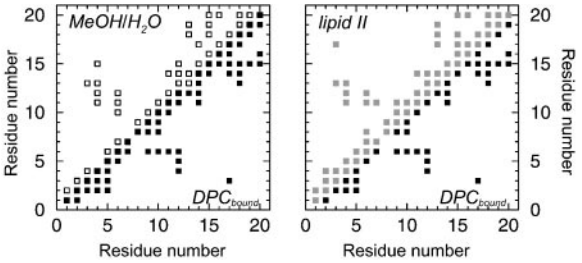

FIG. 5. **NOE contact maps of mersacidin in different sample conditions.** Each *square* corresponds to at least one observed NOE between the two corresponding residues in the $MeOH/H_2O$ mixture (*upper panel* on the *left*), in lipid II-containing DPC micelles (*upper panel* on the right), and in DPC micelles only (*both lower panels*).

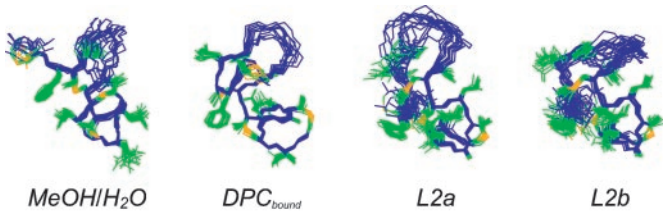

FIG. 6. **Solution NMR structures of mersacidin in various sample conditions.** Only heavy atoms are shown for clarity. Backbone and side chains are shown in *blue* and *green*, respectively; sulfur atoms of the lanthionine rings are shown in *yellow*. $MeOH/H_2O$, free mersacidin in methanol/water mixture; DPC_{bound}, DPC micelle-bound form; L2a and L2b, the two conformations of the lipid II-bound form differing only in the glycine-rich loop (see text for detail). The structures were fitted on backbone heavy atoms within each ensemble, and the various ensembles were aligned using the backbone heavy atoms of residues 13–20.

This suggests that the binding mechanism is based on electrostatic interactions.

DISCUSSION

We have shown that the structure of mersacidin can be substantially modulated by sample conditions. The structures of type B lantibiotics have long been thought to be compact and rigid given the lanthionine ring linkages and their relatively small size in length (8). While the intrinsic flexible nature of the glycine-rich ring gives rise to a higher variability in structure as monitored by ^{15}N relaxation experiments (Fig. 4), which was even observed in the crystal structure (11), mersacidin was, to our surprise, found to possess a minute hinge region (Ala-12 and Abu-13) that can effectively alter the overall backbone geometry by only localized backbone torsion angle changes. Structures obtained from various sample conditions show distinct backbone torsion angle distributions in this region. Furthermore, our results have demonstrated that the chemical shift changes of mersacidin during the course of titration experiments were basically governed by conformational changes. This is rather unusual in the case of protein-protein or protein-ligand interaction studies, making the conventional binding interface mapping approaches inapplicable (42). Multistep titrations and structure determination have revealed the flexible nature of mersacidin and its adaptation to the environment in terms of its three-dimensional structure. Upon binding to lipid II, the structural changes directly affect the exposure of the charge groups suggesting that electrostatic interactions govern the binding mechanism despite the rather hydrophobic nature of mersacidin.

As discussed above, changes in the charge distribution of mersacidin likely play a crucial role in the mersacidin-lipid II interaction. Due to the lack of intermolecular NOEs, there is no sufficient evidence to assess which charge group is mainly responsible for the binding thus far. However, derivatization studies have shown that the methylation of the N terminus increases the minimal inhibitory concentration of mersacidin by 2-fold, and biotinylation makes it inactive. The side chain of Glu-17 has been proposed to be the lipid II binding motif of mersacidin, and replacement of Glu-17 by Ala by mutagenesis makes it inactive.[2] Inactivation is also achieved by amidation of the carboxyl group of Glu-17.[3] These results strongly indicate that these charges are required for the binding. Furthermore the bioactivity is also ion-dependent: the presence of calcium ions can enhance the activity *in vivo*, whereas magnesium ions do not have any effect.[2] Since lipid II is mostly negatively charged (Fig. 1*B*), it is likely that the calcium ion is needed to bridge the Glu-17 side chain to other negatively charged groups of lipid II, unless it forms a direct salt bridge with the positively charged side chain of Lys-3 in lipid II. Should the calcium ion indeed provide a bridge between mersacidin and lipid II, this would explain the lack of intermolecular NOEs (even with long NOESY mixing times up to 500 ms) due to the increased distance between the two, which would exceed a detectable NOE range (>5 Å). Although mersacidin is strongly affected during the course of the titration, little chemical shift changes were observed for lipid II except for the amide proton of γ-Glu-2 (data not shown), suggesting that the non-exchangeable protons of lipid II (Fig. 1*B*) may not be directly involved in binding, whereas the abundant exchangeable hydroxyl protons and/or the pyrophosphate group could play a more important role. It has also been shown that mersacidin can discriminate lipid I from lipid II, indicating that GlcNAc, the only difference between these two, contains part of the recognition motif (6).

Proteins in hydrophobic solvent are thought to retain their native structure as a result of kinetic trapping due to stronger intramolecular hydrogen bonding and a more rigid structure in the absence of water (46). The structure of small peptides like mersacidin can, however, vary remarkably in different envi-

[2] S.-T. D. Hsu, E. Breukink, G. Bierbaum, H.-G. Sahl, B. de Kruijff, R. Kaptein, N. A. J. van Nuland, and A. M. J. J. Bonvin, unpublished results.
[3] W. Dückheimer (Hoechst AG), personal communication.

TABLE II
Structural statistics of mersacidin in different sample environments

	Environments[a]			
	MeOH/H_2O	DPC_{bound}	Lipid II	
			L2a	L2b
Number of structures[b]	12	13	9	8
r.m.s.d. (Å) with respect to the average structure of each ensemble (backbone/heavy)				
Residues 3–4, 12–20	0.27 ± 0.08/0.59 ± 0.0	0.23 ± 0.04/0.44 ± 0.06	0.41 ± 0.11/0.69 ± 0.1	0.44 ± 0.14/0.72 ± 0.16
All	0.90 ± 0.24/0.99 ± 0.1	0.58 ± 0.15/0.64 ± 0.11	0.72 ± 0.11/0.89 ± 0.1	0.79 ± 0.35/0.96 ± 0.27
Number of experimental restraints for structural calculation				
Total NOEs	200	248	241	
Intraresidue NOEs	101	97	111	
Sequential NOEs	59	102	86	
Medium range NOEs	10	16	13	
Long range NOEs	30	33	31	
Dihedral restraints[c]	13	13	13	
Restraint statistic[d]				
NOE r.m.s.d. (10^{-2} Å)	3.30 ± 0.28	2.39 ± 0.75	3.67 ± 0.31	3.76 ± 0.24
Dihedrals r.m.s.d. (°)	1.28 ± 0.19	0.71 ± 0.39	0.69 ± 0.21	0.91 ± 0.30
r.m.s.d. from idealized covalent geometry				
Bonds (Å)	0.0045 ± 0.0002	0.0036 ± 0.0002	0.0046 ± 0.0003	0.0051 ± 0.0002
Angles (°)	0.78 ± 0.04	0.56 ± 0.02	0.74 ± 0.03	0.78 ± 0.04
Impropers (°)	2.1 ± 0.1	1.3 ± 0.1	2.0 ± 0.2	2.2 ± 0.2
Dihedrals (°)	14.3 ± 0.8	13.2 ± 0.8	14.5 ± 0.8	14.7 ± 0.7
CNS energies after water refinement (kcal/mol)				
E_{total}	−386 ± 27	−638 ± 15	−434 ± 25	−407 ± 20
E_{vdw}	−83 ± 19	−96 ± 78	−94 ± 10	−96 ± 4
E_{elec}	−483 ± 13	−642 ± 10	−521 ± 11	−514 ± 7

[a] MeOH/H_2O, free mersacidin in methanol/water mixture solution; DPC_{bound}, mersacidin in DPC micelles; L2a and L2b, two distinct conformations in lipid II-bound form obtained with the same structural restraints.
[b] The number of structures in each condition is obtained from clustering analysis (see "Materials and Methods").
[c] Nine backbone ϕ angles and four side chain χ_1 angles (Ala-12, Leu-14, Glu-17, and Ala-18).
[d] No structure had a violation larger than 0.5 Å for NOE restraints and 5° for dihedral angle restraints.

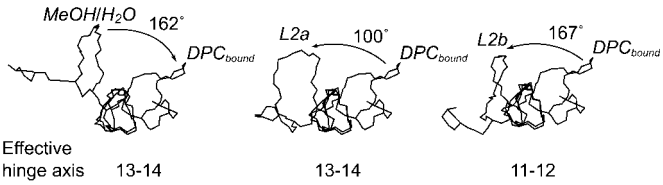

FIG. 7. **Conformational change analysis using the program DynDom (41).** The first two rings are colored in b*lack* for DPC_{bound} and in *gray* for MeOH/H_2O, L2a, and L2b. The rotation of the fragments with respect to the hinge is indicated by an *arrow*. The structures were fitted on backbone heavy atoms of residues 13–20.

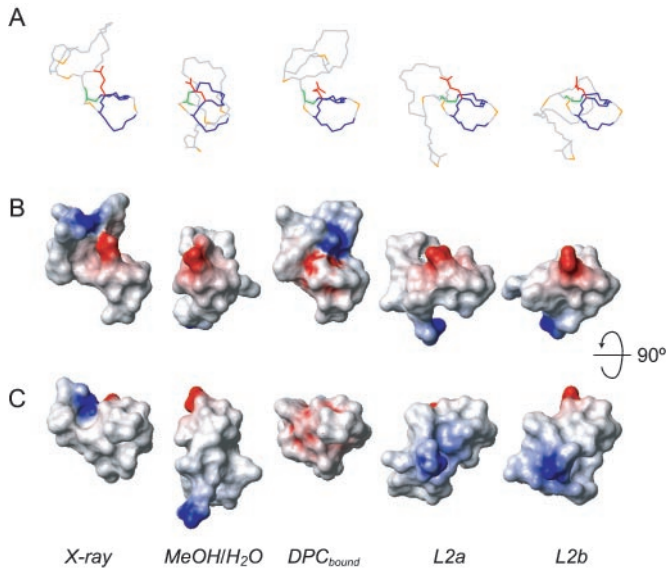

FIG. 8. *A*, representative structures (closest to average) of each structure ensemble. The Glu-17 side chain is shown in *red*. The hinge residue Abu-13 is shown in *green*. The structures were fitted on backbone heavy atoms of residues 13–20 (colored *blue*). The remainder of the structure is shown in *gray*. *B*, surface electrostatic potential of mersacidin in different sample conditions calculated with MOLMOL (40). Positive and negative potentials are colored *blue* and *red*, respectively. The structures are in the same orientation as in *A*. *C*, 90° rotation along the *x* axis of the above structures. The charge distributions reveal the increase of charge accessibility after the addition of lipid II in the hydrophobic DPC micelle solution. The structure of mersacidin in DPC micelles resembles the x-ray structure that was solved in pure methanol.

ronments as has been demonstrated in earlier studies by Kessler and co-workers (47, 48). A compact structure of mersacidin has been observed in the DPC micelle-bound form (DPC_{bound}; our study), in pure methanol solution (10), and in the crystalline state (11) due to the environmental hydrophobicity that is known to facilitate the formation of the intramolecular hydrogen bonds. In the x-ray structure, two hydrogen bonds were identified from the N terminus and the Gly-7 backbone amide to the Glu-17 side chain (11). This is consistent with our finding that the two oppositely charged groups are directed toward each other only in a highly hydrophobic environment in the absence of lipid II. In contrast, in the presence of lipid II, the bound form is clearly distinct from the free form structure as has been shown in this work. Recently the significance of flexibility for bioactivity has been highlighted in the case of the nisin-lipid II interaction (5): a truncation or rigidification of the flexible hinge region substantially abolishes its bioactivity (49). Here mersacidin uses its hinge to adjust the exposure of charges when binding to its "docking molecule," lipid II. We have thus shown in the case of mersacidin that conformational versatility provides a way to adapt to the surrounding environment. It is therefore important, when using static structures of such peptides for structure-based peptide engineering, that the sample conditions be carefully considered.

Many enzymatic functions of proteins require conformational changes during substrate binding and the reaction process. The same is true for the mersacidin-lipid II interaction as observed here when mersacidin binds to DPC micelles and lipid

II. Similar structural changes have been reported by McCafferty and co-workers for ramoplanin (3), a lipoglycodepsipeptide antibiotic, that undergoes a flattening of its structure when it binds to a lipid II analog, UDP-MurNAc-peptapeptide (where MurNAc is *N*-acetylmuramic acid). Ramoplanin is known to be involved in the inhibition of transglycosylation during the biosynthesis of lipid II. It does compete, although not efficiently, with mersacidin for the binding to lipid II (2). Their functionalities are similar in the sense that both peptides recognize specifically parts of lipid II to block cell wall biosynthesis. Notably ramoplanin also shares a topological similarity in structure with mersacidin and actagardine, another type B lantibiotic, although it has no sequence homology with these two lantibiotics (3, 50). From this point of view, conformational changes are evidently a common feature of the lipid II-binding peptides. The structural insights gained here can, therefore, be extended to the type B lantibiotics actagardine (50) and Ala(0)-actagardine (20) since they possess a high degree of sequence homology with mersacidin (the hinge of Ala-12 and Abu-13 is also present in actagardine) (8, 50) and probably to other lipid II-binding peptides, like ramoplanin, as well.

Acknowledgment—We thank C. Szekat (Institute of Medical Microbiology and Immunology, University of Bonn) for expert technical assistance in the purification of mersacidin.

REFERENCES

1. Zasloff, M. (2002) *Nature* **415,** 389–395
2. Brötz, H., Josten, M., Wiedemann, I., Schneider, U., Götz, F., Bierbaum, G., and Sahl, H.-G. (1998) *Mol. Microbiol.* **30,** 317–327
3. Cudic, P., Kranz, J. K., Behenna, D. C., Kruger, R. G., Tadesse, H., Wand, A. J., Veklich, Y. I., Weisel, J. W., and McCafferty, D. G. (2002) *Proc. Natl. Acad. Sci. U. S. A.* **99,** 7384–7389
4. Nagarajan, R. (1993) *J. Antibiot.* (*Tokyo*) **46,** 1181–1195
5. Breukink, E., Wiedemann, I., van Kraaij, C., Kuipers, O. P., Sahl, H.-G., and de Kruijff, B. (1999) *Science* **286,** 2361–2364
6. Brötz, H., Bierbaum, G., Leopold, K., Reynolds, P. E., and Sahl, H.-G. (1998) *Antimicrob. Agents Chemother.* **42,** 154–160
7. Brötz, H., Bierbaum, G., Reynolds, P. E., and Sahl, H.-G. (1997) *Eur. J. Biochem.* **246,** 193–199
8. Brötz, H., and Sahl, H.-G. (2000) *J. Antimicrob. Chemother.* **46,** 1–6
9. Jack, R. W., and Jung, G. (2000) *Curr. Opin. Chem. Biol.* **4,** 310–317
10. Prasch, T., Naumann, T., Markert, R. L., Sattler, M., Schubert, W., Schaal, S., Bauch, M., Kogler, H., and Griesinger, C. (1997) *Eur. J. Biochem.* **244,** 501–512
11. Schneider, T. R., Karcher, J., Pohl, E., Lubini, P., and Sheldrick, G. M. (2000) *Acta Crystallogr. Sect. D Biol. Crystallogr.* **56,** 705–713
12. Opella, S. J. (1997) *Nat. Struct. Biol.* **4,** 845–848
13. Opella, S. J., Ma, C., and Marassi, F. M. (2001) *Methods Enzymol.* **339,** 285–313
14. Bader, R., Bettio, A., Beck-Sickinger, A. G., and Zerbe, O. (2001) *J. Mol. Biol.* **305,** 307–329
15. Neidigh, J. W., Fesinmeyer, R. M., Prickett, K. S., and Andersen, N. H. (2001) *Biochemistry* **40,** 13188–13200
16. Williams, K. A., Farrow, N. A., Deber, C. M., and Kay, L. E. (1996) *Biochemistry* **35,** 5145–5157
17. Kutateladze, T., and Overduin, M. (2001) *Science* **291,** 1793–1796
18. Hsu, S.-T., Breukink, E., de Kruijff, B., Kaptein, R., Bonvin, A. M. J. J., and van Nuland, N. A. J. (2002) *Biochemistry* **41,** 7670–7676
19. Bierbaum, G., Brötz, H., Koller, K. P., and Sahl, H.-G. (1995) *FEMS Microbiol. Lett.* **127,** 121–126
20. Vertesy, L., Aretz, W., Bonnefoy, A., Ehlers, E., Kurz, M., Markus, A., Shiell, M., Vogel, M., Wink, J., and Kogler, H. (1999) *J. Antibiot.* (*Tokyo*) **52,** 730–741
21. Cavanagh, J., Fairbrother, W. J., Palmer, A. G., III, and Skelton, N. J. (1996) *Protein NMR Spectroscopy*, 1st Ed., Academic Press, San Diego, CA
22. Ludvigsen, S., Andersen, K. V., and Poulsen, F. M. (1991) *J. Mol. Biol.* **217,** 731–736
23. Nilges, M., Clore, G. M., and Gronenborn, A. M. (1990) *Biopolymers* **29,** 813–822
24. Xu, R. X., Olejniczak, E. T., and Fesik, S. W. (1992) *FEBS Lett.* **305,** 137–143
25. Basus, V. J. (1989) *Methods Enzymol.* **177,** 132–149
26. Delaglio, F., Grzesiek, S., Vuister, G. W., Zhu, G., Pfeifer, J., and Bax, A. (1995) *J. Biomol. NMR* **6,** 277–293
27. Johnson, B. A., and Blevins, R. A. (1994) *J. Biomol. NMR* **4,** 603–614
28. Wymore, T., Gao, X. F., and Wong, T. C. (1999) *J. Mol. Struct.* **486,** 195–210
29. Marrink, S. J., Tieleman, D. P., and Mark, A. E. (2000) *J. Phys. Chem. B* **104,** 12165–12173
30. Farrow, N. A., Muhandiram, R., Singer, A. U., Pascal, S. M., Kay, C. M., Gish, G., Shoelson, S. E., Pawson, T., Forman-Kay, J. D., and Kay, L. E. (1994) *Biochemistry* **33,** 5984–6003
31. Dayie, K. T., Wagner, G., and Lefevre, J. F. (1996) *Annu. Rev. Phys. Chem.* **47,** 243–282
32. Anglister, J., Grzesiek, S., Ren, H., Klee, C. B., and Bax, A. (1993) *J. Biomol. NMR* **3,** 121–126
33. Wand, A. J., Ehrhardt, M. R., and Flynn, P. F. (1998) *Proc. Natl. Acad. Sci. U. S. A.* **95,** 15299–15302
34. Wilkins, D. K., Grimshaw, S. B., Receveur, V., Dobson, C. M., Jones, J. A., and Smith, L. J. (1999) *Biochemistry* **38,** 16424–16431
35. Brünger, A. T., Adams, P. D., Clore, G. M., DeLano, W. L., Gros, P., Grosse-Kunstleve, R. W., Jiang, J. S., Kuszewski, J., Nilges, M., Pannu, N. S., Read, R. J., Rice, L. M., Simonson, T., and Warren, G. L. (1998) *Acta Crystallogr. Sect. D Biol. Crystallogr.* **54,** 905–921
36. Nilges, M., and Donoghue, S. I. (1998) *Prog. Nucl. Magn. Reson. Spectrosc.* **32,** 107–139
37. Linge, J. P., O'Donoghue, S. I., and Nilges, M. (2001) *Methods Enzymol.* **339,** 71–90
38. Linge, J., Williams, M. A., Spronk, C. A. E. M., Bonvin, A. M. J. J., and Nilges, M. (2003) *Proteins Struct. Funct. Genet.* **50,** 496–506
39. Bonvin, A. M. J. J., Houben, K., Guenneugues, M., Kaptein, R., and Boelens, R. (2001) *J. Biomol. NMR* **21,** 221–233
40. Koradi, R., Billeter, M., and Wüthrich, K. (1996) *J. Mol. Graph.* **14,** 51–55
41. Feenstra, K. A., Hess, B., and Berendsen, H. J. C. (1999) *J. Comput. Chem.* **20,** 786–798
42. Zuiderweg, E. R. (2002) *Biochemistry* **41,** 1–7
43. Kay, L. E. (1998) *Nat. Struct. Biol.* **5,** (suppl.) 513–517
44. Palmer, A. G., III (1997) *Curr. Opin. Struct. Biol.* **7,** 732–737
45. Pamler, A. G., III (2001) *Annu. Rev. Biophys. Biomol. Struct.* **30,** 129–155
46. Mattos, C., and Ringe, D. (2001) *Curr. Opin. Struct. Biol.* **11,** 761–764
47. Kessler, H., Mierke, D. F., Saulitis, J., Seip, S., Steuernagel, S., Wein, T., and Will, M. (1992) *Biopolymers* **32,** 427–433
48. Kessler, H., Haessner, R., and Schuler, W. (1993) *Helv. Chim. Acta* **76,** 117–130
49. Wiedemann, I., Breukink, E., van Kraaij, C., Kuipers, O. P., Bierbaum, G., de Kruijff, B., and Sahl, H.-G. (2001) *J. Biol. Chem.* **276,** 1772–1779
50. Zimmermann, N., and Jung, G. (1997) *Eur. J. Biochem.* **246,** 809–819

NMR Study of Mersacidin and Lipid II Interaction in Dodecylphosphocholine Micelles: CONFORMATIONAL CHANGES ARE A KEY TO ANTIMICROBIAL ACTIVITY

Shang-Te D. Hsu, Eefjan Breukink, Gabriele Bierbaum, Hans-Georg Sahl, Ben de Kruijff, Rob Kaptein, Nico A. J. van Nuland and Alexandre M. J. J. Bonvin

J. Biol. Chem. 2003, 278:13110-13117.
doi: 10.1074/jbc.M211144200 originally published online January 31, 2003
